

A 'loop recapture' mechanism for ACF-dependent nucleosome remodeling

Ralf Strohner¹, Malte Wachsmuth², Karoline Dachauer¹, Jacek Mazurkiewicz², Julia Hochstatter¹, Karsten Rippe² & Gernot Längst¹

The ATPase ISWI is the molecular motor of several nucleosome remodeling complexes including ACF. We analyzed the ACF-nucleosome interactions and determined the characteristics of ACF-dependent nucleosome remodeling. In contrast to ISWI, ACF interacts symmetrically with DNA entry sites of the nucleosome. Two-color fluorescence cross-correlation spectroscopy measurements show that ACF can bind four DNA duplexes simultaneously in a complex that contains two Acf1 and ISWI molecules. Using bead-bound nucleosomal substrates, nucleosome movement by mechanisms involving DNA twisting was excluded. Furthermore, an ACF-dependent local detachment of DNA from the nucleosome was demonstrated in a novel assay based on the preferred intercalation of ethidium bromide to free DNA. The findings suggest a loop recapture mechanism in which ACF introduces a DNA loop at the nucleosomal entry site that propagates over the histone octamer surface and leads to nucleosome repositioning.

Changes in chromatin structure induced by chromatin remodeling complexes modulate the access of regulatory proteins to DNA. Therefore, chromatin remodelers are involved in the regulation of all DNA-dependent processes, like transcription, replication and recombination^{1,2}. In the current models for nucleosome mobility not all histone-DNA interactions are broken simultaneously. Nucleosome movements were first explained by the 'twist diffusion model,' which suggests that thermal energy fluctuations would be sufficient to twist the DNA helix at the edge of the nucleosomes, replacing histone-DNA interactions by neighboring DNA base pairs. The additional base pairs within the nucleosome would be propagated over the histone-octamer surface, changing the translational position of the nucleosome^{3,4}. According to this model, the DNA is rotated around its axis as it 'screws' over the surface of the nucleosome. Alternatively, it was proposed that nucleosomes are repositioned according to the 'loop recapture' model⁵⁻⁷. Thermal energy would lead to the detachment of a segment of DNA at the entry site of the nucleosome⁸. Dissociation of a DNA segment and interaction of the freed protein surfaces with neighboring DNA segments would lead to the formation of a DNA loop on the histone octamer^{9,10}. The propagation of the DNA loop over the histone octamer would change the translational position of the nucleosome, corresponding to the size of the DNA loop⁵.

Chromatin remodeling refers to numerous ATP-dependent changes within a chromatin substrate. The different classes of chromatin remodeling complexes exhibit distinct activities in *in vitro* remodeling assays, which all involve the relocation of nucleosomes on DNA². However, the remodeling mechanism itself is still not understood. Our studies focus on *Drosophila melanogaster* ISWI, the molecular

motor of NURF¹¹, ACF¹² and CHRAC¹³. Here we examined the remodeling mechanism of ACF, which contains ISWI and the Acf1 subunit¹⁴.

Remodeling complexes have been shown to introduce superhelical torsion into nucleosomal DNA, suggesting a twisting mechanism¹⁵. However, the activity of the complexes tested so far is not affected by nicked DNA or DNA extrusions, which should inhibit nucleosome mobility according to the DNA twisting mechanism¹⁶⁻¹⁸. This observation suggests remodeling occurs via propagation of a segment of detached DNA, independent from the integrity of the phosphodiester backbone. In addition, ISWI-dependent nucleosome mobility has been facilitated by the introduction of specific DNA nicks located at the site of ISWI-nucleosome interaction¹⁸. This finding may result from the increased DNA flexibility, which reduces the energy requirement for DNA bending during loop formation.

In this study, we addressed the ACF-nucleosome topology and investigated the basis of the nucleosome remodeling mechanism. In contrast to ISWI alone, ACF binds symmetrically to the DNA entry site, interacting with the nucleosome and adjacent linker DNA. We showed by fluorescence correlation (FCS) and fluorescence cross-correlation spectroscopy (FCCS) that ACF consists of two Acf1 and two ISWI molecules, capable of binding four DNA molecules simultaneously. DNA twisting is not involved in the nucleosome remodeling process, as nucleosomes reconstituted on biotinylated DNA and fixed to magnetic beads were efficiently remodeled by ACF. We detected increased DNA accessibility in the nucleosome upon ACF binding and propose the loop recapture model as the basic mechanism for ACF-dependent nucleosome remodeling.

¹Adolf-Butenandt-Institut, Molekularbiologie, Schillerstrasse 44, 80336 München, Germany. ²Kirchhoff-Institut für Physik, AG Molekulare Biophysik, Im Neuenheimer Feld 227, 69120 Heidelberg, Germany. Correspondence should be addressed to G.L. (laengst@lmu.de).

Published online 17 July 2005; doi:10.1038/nsmb966

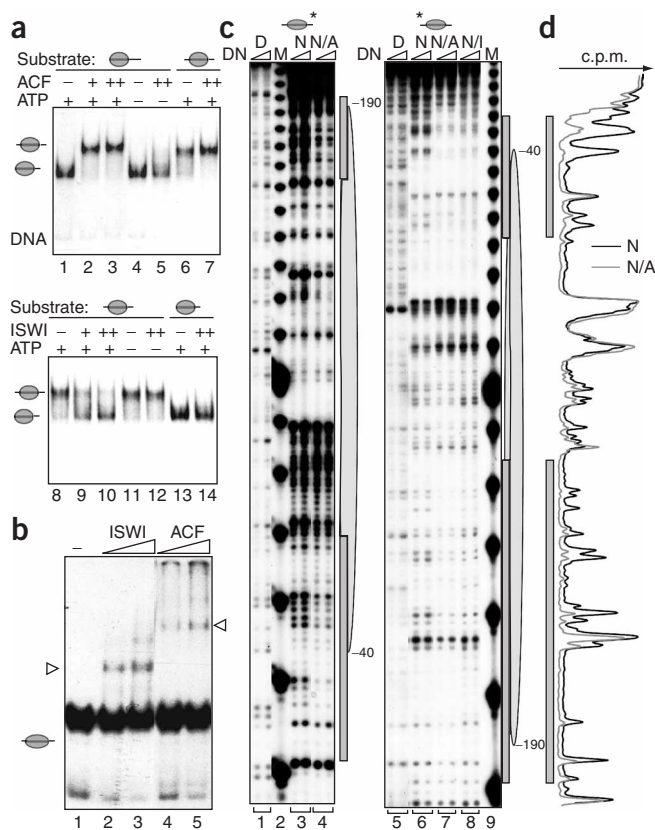


Figure 1 ACF interacts with the DNA entry site of the nucleosome. (a) Nucleosomes positioned at the border or the center of the 248-bp rDNA fragment (60 fmol) were incubated with ACF (+, 2 fmol; ++, 6 fmol) or ISWI (+, 2 fmol; ++, 6 fmol), in the presence or absence of ATP, as indicated. Changes in nucleosome positioning were analyzed by native PAGE. The nucleosomal substrates for the remodeling reactions are at the top of the panels. Nucleosomes positioned at the center or border of the DNA fragment are ellipses with protruding DNA. (b) ISWI and ACF form distinct nucleosome-remodeler complexes. Increasing amounts of ISWI and ACF (10 and 20 fmol) were incubated with nucleosomes (60 fmol) positioned at the center of the 248-bp DNA fragment. Nucleosome-remodeler complexes are marked with arrowheads. (c) ACF interacts symmetrically with the entry site of the nucleosome. Purified nucleosomes (N) or DNA (D) radioactively labeled at position +16 (panels 1–4) or labeled at position –232 (panels 5–8) were incubated with ACF (N/A) or ISWI (N/I) as indicated. DNase I-treated free DNA (D), nucleosomes (N) and nucleosome-remodeler complexes were resolved by native PAGE. The nucleosomes and the nucleosome-remodeler complexes were excised, and the DNA was isolated and analyzed on sequencing gels. Lanes corresponding to DNA (panels 1 and 5), nucleosomes (panels 3 and 6), nucleosome-ACF complexes (panels 4 and 7), nucleosome-ISWI complexes (panel 8) and the 10-bp DNA ladder (M; lanes 2 and 9) are indicated. The localization of the nucleosome (gray ellipse) and ACF-dependent protections (boxes) are indicated. (d) Phosphoimager scan of the nucleosome and nucleosome-ACF complex footprinting pattern (low DNase I concentrations of c, panels 6 and 7). The nucleosomal pattern is black and the nucleosome-ACF pattern is gray. Gray boxes indicate ACF-dependent protections.

RESULTS

Symmetric ACF-nucleosome interactions

We recently established an assay to monitor mononucleosome movement catalyzed by ATP-dependent nucleosome remodeling factors¹⁹. The wrapping of short DNA fragments around histone octamers frequently leads to multiple translational positions that can be separated and stably isolated after native gel electrophoresis. As shown previously, recombinant ISWI moves centrally located nucleosomes toward fragment ends¹⁹ (Fig. 1a, lanes 8–14). In contrast, ACF moves the nucleosomes from the end of the DNA fragment to more central positions^{18,20} (Fig. 1a, lanes 1–7).

To understand the nature of the different remodeling modes, we compared the nucleosome-binding characteristics of ISWI and ACF in electromobility shift assays (EMSA). Incubation of the centrally positioned nucleosome with ACF and ISWI resulted in the formation of specific nucleosome-remodeler complexes (Fig. 1b). As expected for its higher molecular mass, the ACF-nucleosome complex migrated slower than the ISWI-nucleosome complex. To compare the topology of ISWI-nucleosome and ACF-nucleosome interactions, we carried out footprinting experiments. Positioned nucleosomes were incubated with ISWI or ACF to allow formation of complex. These were treated mildly with DNase I and separated by gel electrophoresis. DNA fragments corresponding to free DNA, nucleosomal DNA and to the ISWI-nucleosome or ACF-nucleosome complex were purified from the gel and analyzed on denaturing polyacrylamide gels.

Partial DNase I digestion of the nucleosomal DNA resulted in a characteristic cleavage pattern that differed from free DNA (Fig. 1c, compare lanes 1 and 3; 5 and 6). ACF protected nucleosomal and linker DNA at the DNA entry site of the nucleosome without altering the histone-DNA interactions in the central part of the nucleosome

(Fig. 1c, compare panels 3 and 4; 6 and 7). A quantitative analysis of the DNase I footprinting pattern revealed that ACF protected the DNA at entry site up to ten-fold (Fig. 1d). This protection pattern argues for simultaneous binding of ACF to the entry site of the nucleosome and is not compatible with a mixture of species in which ACF is bound only to either the incoming or outgoing DNA. Thus, ACF interacted symmetrically with ~40 base pairs (bp) of the nucleosomal DNA at the DNA entry site and the adjacent linker DNA. In contrast, ISWI interacted only on one side of the nucleosome (Fig. 1c, panel 8), leaving the other side unprotected¹⁸.

ACF has four DNA-binding sites

The DNA binding of ACF and of the isolated ISWI subunit was studied with a 59-bp DNA (ES-2 duplex) by FCS and FCCS. With this method the composition and mobility of individual protein-DNA complexes can be evaluated^{21–24}. Duplexes labeled at the 5' end with 6-carboxyfluorescein (ES-2_f carrying FAM) or 6-carboxy-X-rhodamine (ES-2_r carrying ROX) or as a reference with both dyes (ES-2_{fr}) were used. The amount of particles carrying both dyes simultaneously is derived from the ratio of cross-correlation and autocorrelation amplitudes (see **Supplementary Methods** online). The instrumental setup was calibrated with reference samples that contained increasing amounts of double-labeled ES-2_{fr} mixed with the single-labeled ES-2_f and ES-2_r. The results demonstrate that the FCCS signal accurately reflects the amount of particles carrying both fluorophores (Fig. 2a,b)^{22,23}. To examine whether the ACF complex can bind multiple DNA duplexes simultaneously, a sample containing an equimolar mixture of ES-2_f and ES-2_r was titrated with ACF (Fig. 2c,d). The concentration of ACF is given in terms of an ACF monomer complex consisting of one ISWI and Acl1 subunit. The 1:1 stoichiometry of the two subunits is based on quantification of Coomassie-stained SDS gels, in which a ratio of 1.4 ± 0.2 for both proteins was determined, which agrees with the expected ratio of 1.43 based on the molecular masses of 170 kDa (Acl1) and 119 kDa

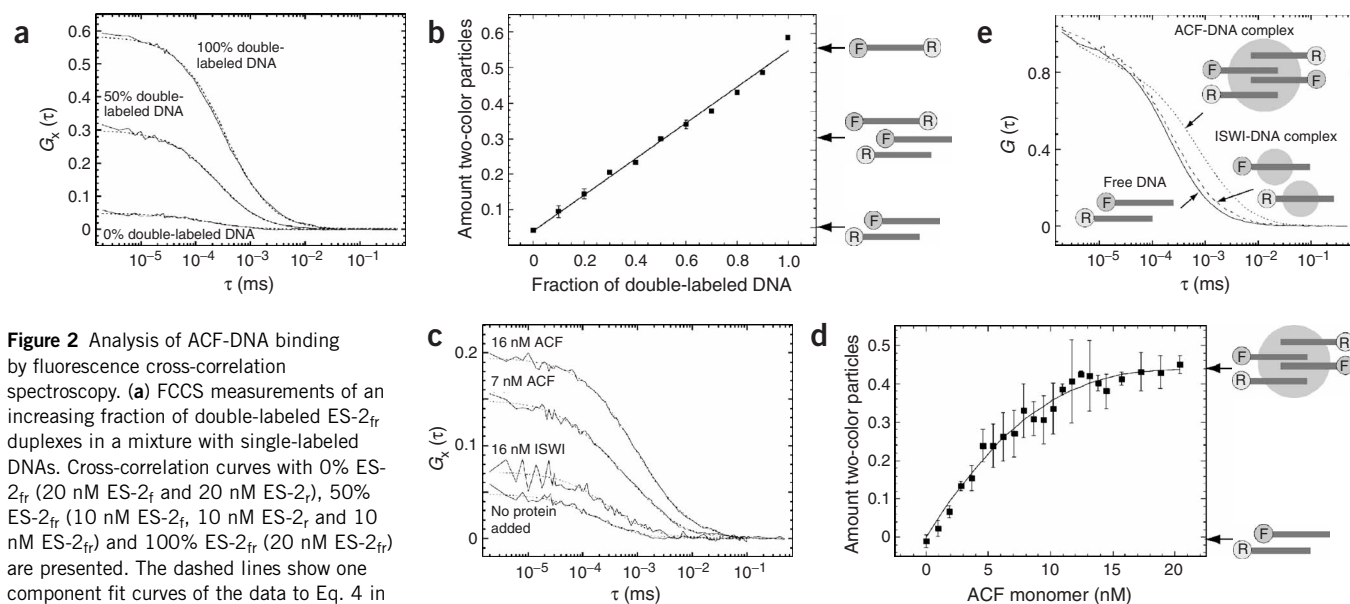


Figure 2 Analysis of ACF-DNA binding by fluorescence cross-correlation spectroscopy. **(a)** FCCS measurements of an increasing fraction of double-labeled ES-2_{fr} duplexes in a mixture with single-labeled DNAs. Cross-correlation curves with 0% ES-2_{fr} (20 nM ES-2_f and 20 nM ES-2_r), 50% ES-2_{fr} (10 nM ES-2_f, 10 nM ES-2_r and 10 nM ES-2_{fr}) and 100% ES-2_{fr} (20 nM ES-2_{fr}) are presented. The dashed lines show one component fit curves of the data to Eq. 4 in the **Supplementary Methods**. **(b)** FCCS signals for different ratios of the double-labeled ES-2_{fr} duplex to single-labeled DNAs. The measured *ratioG* versus the fraction of double-labeled duplex ES-2_{fr} as given by $[\text{ES-2}_{fr}] / ([\text{ES-2}_f] + [\text{ES-2}_{fr}])$ or $[\text{ES-2}_{fr}] / ([\text{ES-2}_f] + [\text{ES-2}_{fr}])$ is plotted. **(c)** FCCS measurements of ACF and ISWI binding to the ES-2 DNA duplex. Samples containing a mixture of 20 nM ES-2_f and 20 nM ES-2_r were titrated with ACF protein. Cross-correlation curves of ACF-DNA at 7 and 16 nM ACF monomer and ISWI-DNA complexes at 16 nM ISWI are shown. The dashed lines show one component fit curves to Eq. 4 (**Supplementary Methods**). **(d)** The corrected *ratioG_{cor}* is plotted versus the concentration of ISWI or Acf1 subunits in ACF according to the analysis described in the **Supplementary Methods**. The solid line represents the least squares fit curve to Eqs. S9 and S11 (**Supplementary Methods**) yielding $k = 2.3 \pm 0.8$ ISWI and Acf1 subunits, $n = 4.3 \pm 0.4$ DNA binding sites per ACF complex and a K_d of 10 ± 8 nM per isolated binding site. **(e)** Normalized autocorrelation curves of the ROX channel are shown for a sample of 20 nM ES-2_f and 20 nM ES-2_r duplex in the absence of ACF and after addition of ACF to an ISWI-Acf1 subunit concentration of 16 nM or ISWI to a concentration of 16 nM are shown. The FAM channel showed equivalent results.

(ISWI). The FCCS data of ACF-DNA complexes revealed a cross-correlation signal with a value of 0.45 ± 0.02 at the highest ACF concentrations studied (**Fig. 2d**), where according to the autocorrelation function some free DNA ($\sim 30\%$) was present. The theoretical maximum value for a complex that has $n = 2$ binding sites is 0.33 (**Supplementary Methods**). Thus, the cross-correlation signal clearly demonstrates that the ACF complex can bind more than two ES-2 duplexes.

A detailed analysis of the results presented in **Figure 2d** including the autocorrelation functions (**Fig. 2e**) is described in **Supplementary Methods**. The least-squares fit to a theoretical description yielded 2.3 ± 0.8 ISWI and Acf1 subunits and 4.3 ± 0.4 DNA-binding sites per ACF complex and microscopic dissociation constant $K_d = 10 \pm 8$ nM for an isolated binding site (**Fig. 2d**, solid line).

At a concentration of 16 nM ISWI, the FCCS signal was only slightly higher than the DNA background signal of the singly labeled DNA strands in the absence of protein (**Fig. 2c**). Thus, ISWI alone could not bind two or more DNA strands simultaneously under the experimental conditions studied. The FCS-FCCS analysis of ISWI-DNA complexes was hindered by a nonspecific aggregation of ISWI with DNA, which was observed with increasing protein concentrations. This effect was not present with ACF and could not be eliminated by varying buffer conditions or DNA length. Thus, for the FCS-FCCS experiments, only fluorescence signals from single protein-DNA complexes were used for the evaluation. The large nonspecific ISWI-DNA aggregates typically contained more than ten fluorophores and could be clearly distinguished from specific ISWI-DNA complexes.

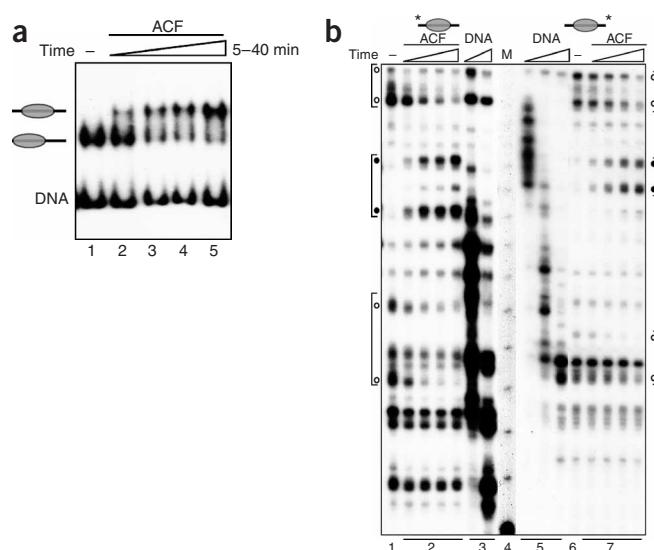
The diffusion time of the ES-2_{fr} DNA determined from a one component fit of the cross-correlation curves was 0.24 ± 0.02 ms,

which corresponds to a diffusion coefficient of $D_{20,w} = 5.3 \times 10^{-7} \text{ cm}^2 \text{ s}^{-1}$ (ref. 25). For the ACF complex with bound ES-2_f and ES-2_r a diffusion time of 0.97 ± 0.05 ms was obtained from which $D_{20,w} = (1.4 \pm 0.1) 10^{-7} \text{ cm}^2 \text{ s}^{-1}$ is computed with the DNA reference value. The corresponding diffusion time for the ISWI-DNA complex was estimated to be around 0.30–0.40 ms from the autocorrelation curves under conditions in which a substantial amount of free DNA was still present (**Fig. 2e**). It would correspond to diffusion coefficient values of $3 \times 10^{-7} \text{ cm}^2 \text{ s}^{-1}$ to $4 \times 10^{-7} \text{ cm}^2 \text{ s}^{-1}$ but the presence of a substantial fraction of free DNA prevented an accurate determination of this parameter. The diffusion coefficient measured here for the ACF complex was considerably lower than the value of $D_{20,w} = 2.5 \times 10^{-7} \text{ cm}^2 \text{ s}^{-1}$ determined previously for a protein complex of 433 kDa with two bound ES-2 duplexes²⁵. Thus, it is indicative for the formation of a larger size ACF complex and would be consistent with an ACF heterotetramer in an extended conformation with four DNA duplexes bound. In agreement with the FCS-FCCS data analysis an apparent molecular mass of 600–700 kDa for ACF in the absence of DNA was derived from size-exclusion chromatography and glycerol gradients (see **Supplementary Fig. 1** online).

Nucleosomes apparently move in large steps

The models for nucleosome remodeling predict nucleosome movement either by single base pairs or in larger steps according to the DNA loop size. If nucleosomes occupy multiple intermediate positions during their remodeling reaction, it should be possible to predict the remodeling mechanism from their movement behavior.

Figure 3 High-resolution analysis of the nucleosome remodeling reaction. (a) Nucleosomes positioned at the end of the DNA fragment (lane 1) were incubated with ACF and ATP. The remodeling reactions were stopped after 5, 10, 20 and 40 min (lanes 2–5) by the addition of competitor DNA. Nucleosome positions were analyzed by native gel electrophoresis. (b) ExoIII mapping of nucleosome positions. Aliquots of the remodeling reaction in a, with nucleosomes radioactively labeled at position –232 of the DNA (panel 1–3) and of a remodeling reaction labeled at position +16 of the DNA (panel 5–7), were analyzed by ExoIII footprinting. Nucleosomes were digested with 400 U ml⁻¹ of ExoIII for 2 min at 30 °C and the purified DNA was analyzed on sequencing gels. Panels 3 and 5 show the ExoIII digestion kinetics of free DNA. DNA was digested for 10 and 20 s (panel 3) and 10 to 40 s (panel 5) with 400 U ml⁻¹ of ExoIII. Free DNA was fully digested after 2 min (data not shown). The DNA marker (M; 10-bp ladder) is shown in panel 4. Open circles indicate the start positions of the nucleosomes at the borders of the DNA fragment and closed circles indicate the final nucleosome positions.



We mapped the ACF-dependent nucleosome remodeling intermediates in nucleotide resolution by exonuclease III (ExoIII) digestion. Purified nucleosomes positioned at the border of the 248-bp rDNA fragment were incubated with ACF and ATP. After 5, 10, 20 and 40 min the reactions were stopped and subsequently analyzed by electromobility shift assay and ExoIII digestion (Fig. 3). With increasing time, nucleosomes were quantitatively moved from the end position to a central position on the rDNA fragment as visualized by the nucleosome sliding assay (Fig. 3a). Accordingly, we observed nucleosome movement by ExoIII footprinting, in which ExoIII pause sites define nucleosome boundaries (Fig. 3b). Nucleosomes located at the end of the DNA fragment disappeared with increasing time and were replaced by nucleosomes positioned at the center of the rDNA fragment. In this reaction nucleosomes moved ~50 bp without visible intermediates. Such behavior would suggest a looping mechanism. However, it is also possible that a twisting mechanism faster than the experiment's time resolution would lead to similar results.

ACF moves nucleosomes coupled to beads

To exclude a twisting mechanism, we generated modified nucleosomes with a large obstacle in the path of the nucleosome remodeling reaction. In case of a DNA-twisting mechanism, an obstacle (a magnetic bead) within the nucleosome is expected to destroy the nucleosome, as DNA rotation requires the obstacle to pass the freed space between the DNA and the histone octamer surface.

Using PCR we generated DNA fragments harboring one or two biotin molecules close to the center of the DNA fragments (Fig. 4a,b). The biotin molecules are positioned such that any nucleosome on the DNA fragments of 236 or 248 bp would carry a biotin on its surface. Nucleosomes assembled on the DNA fragment carrying two biotin molecules did not hinder ACF-dependent nucleosome remodeling (Fig. 4c). Biotin and its linker present a flexible moiety that may not hamper a DNA rotation-based remodeling reaction. To exclude any DNA rotation we assembled nucleosomes on a DNA fragment carrying one biotin close to its center. The end-positioned nucleosomes were purified and coupled to magnetic beads. Nucleosome remodeling was carried out on free nucleosomes and nucleosomes coupled to beads. The nucleosome positions were determined by ExoIII digestion, revealing the nucleosome boundaries (Fig. 4d). Nucleosome remodeling was not affected by the free biotin moiety, and ACF moved nucleosomes from the DNA ends to central positions (lanes 1–3). Coupling of the positioned nucleosomes to magnetic beads did not affect nucleosome positioning and notably, nucleosome remodeling was not impaired (lanes 4–6). In the presence of ATP, ACF

relocated bead-bearing nucleosomes to central positions (lane 6). Similar nucleosome positions were occupied in the free and bead-bound nucleosomes. Nucleosomes were not disrupted, because protein-free DNA would have been completely digested in the time frame of the experiment (lanes 8 and 9). In addition, ACF dependent nucleosome remodeling did not involve transient uncoupling of the nucleosomes from the streptavidin beads (Supplementary Fig. 2 online). These results suggest that ACF-dependent nucleosome remodeling does not involve DNA rotation as a driving force.

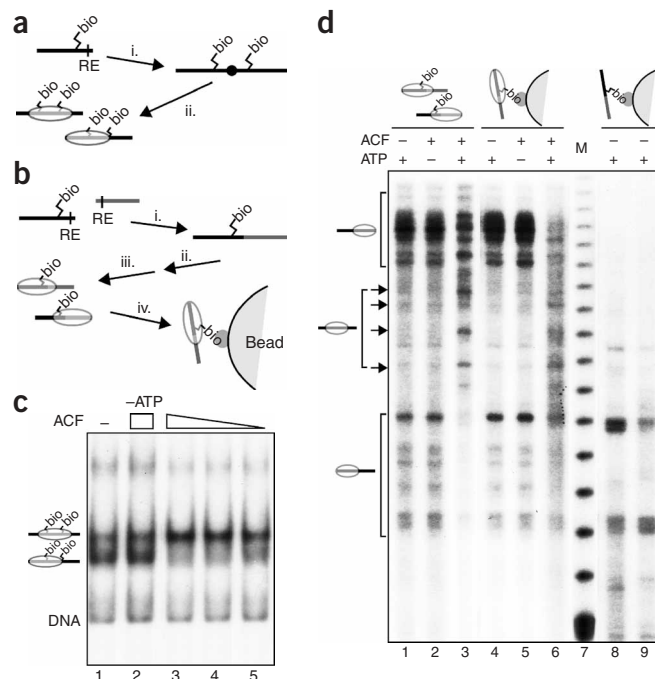
ACF generates accessible nucleosomal DNA

The experiments above suggest a looping mechanism for ACF-dependent nucleosome remodeling. The loop recapture model predicts the generation of accessible DNA in the realm of the nucleosome. To test this hypothesis we exploited the preferential intercalation of ethidium bromide (EB) into free DNA as compared with nucleosomal DNA^{26,27}. The site-specific intercalation of EB can be analyzed by laser-induced crosslinking, which creates single-strand breaks at the intercalation site^{28,29}. Analyzing nucleosome remodeling in the presence of EB should therefore allow detection of accessible DNA regions in the nucleosome.

Irradiation of DNA–EB complexes with a 488-nm laser resulted in decreased EB absorption at 510 nm and corresponding increase in absorption at 420 nm (Fig. 5a). Dye bleaching in this reaction is directly coupled to DNA cleavage³⁰. Irradiation of nucleosomes for up to 80 min did not affect the structure or stability of the nucleosome particles, as judged by native gel electrophoresis (Fig. 5b). EB did not interfere with the nucleosome stability or the ACF-dependent nucleosome remodeling reaction when applied in concentrations $\leq 10^{-6}$ M (Fig. 5c). Nucleosomes were efficiently remodeled until the EB concentration was increased above 10^{-5} M, leading to disruption of the nucleosome (lanes 2–6). Disruption was not dependent on active remodeling, as EB had the same effect in absence of ACF and ATP (lanes 7–11). All subsequent nucleosome remodeling reactions were done at an EB concentration of 5×10^{-7} M, which did not affect nucleosome remodeling and nucleosome integrity.

To detect site-specific DNA loop formation rather than a general increase of DNA accessibility we used nucleosomes assembled on 146 bp of DNA and purified nucleosomes positioned at the center of the 248-bp rDNA fragment. These nucleosomes were not moved by

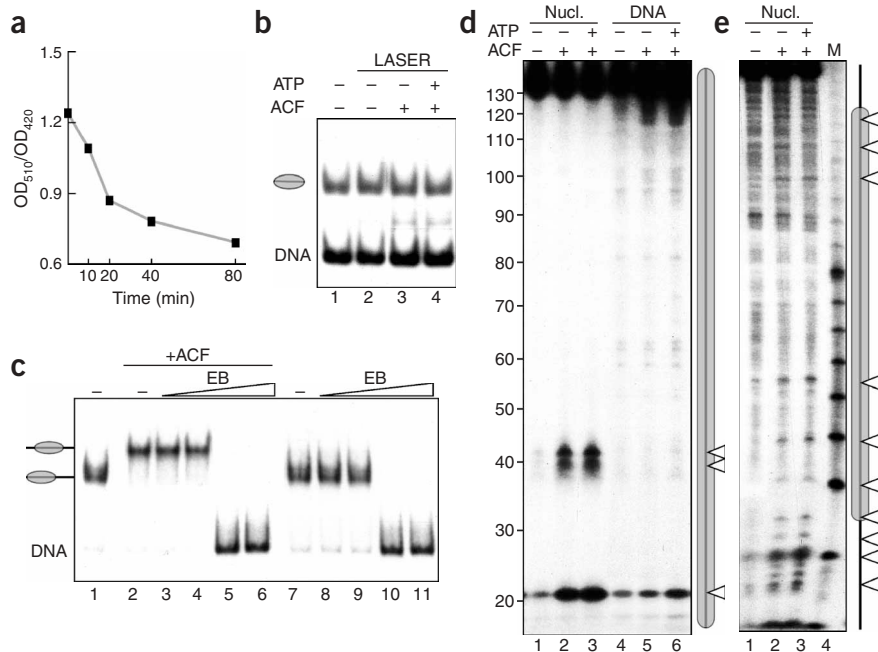
Figure 4 Large obstacles do not inhibit nucleosome remodeling. **(a)** Scheme showing the preparation of nucleosomes, harboring two biotin moieties at the center of the DNA fragment. DNA containing one biotin moiety close to the end was generated by PCR. The DNA was cleaved with BamHI and ligation resulted in a DNA fragment containing two biotin moieties close to the center, spaced by 44 bp (i). The radioactively labeled DNA was gel-purified and assembled into nucleosomes (ii). **(b)** Scheme showing the preparation of the biotinylated DNA and positioned nucleosomes coupled to magnetic beads. Two DNA fragments, of which one was carrying a biotin moiety close to one end and the radioactive label at the other end, were generated by PCR. DNAs were cleaved with BamHI, mixed and ligated. The DNA fragment harboring only one biotin moiety in the center of the DNA fragment was gel-purified (i). Nucleosomes were reconstituted (ii), and laterally positioned nucleosomes were isolated (iii) and coupled to magnetic beads (iv). **(c)** Nucleosomes assembled on the DNA fragment carrying two biotin moieties were incubated with ACF (5–45 fmol) in the presence and absence of ATP, as indicated. Nucleosome positions were resolved on native polyacrylamide gels. DNA and nucleosome positions are indicated at left. **(d)** ExoIII analysis of nucleosome positions. Nucleosomes positioned at the border of the DNA fragment carrying one biotin moiety were analyzed in solution (lanes 1–3) or when coupled to magnetic beads (lanes 4–6). Nucleosomes (lanes 1–6) and free DNA coupled to beads (lanes 8 and 9) were incubated with ATP and ACF as indicated and digested with 400 U ml⁻¹ of ExoIII for 3 min at 26 °C. Protein-free DNA was digested for 1 min (lane 8) or 3 min (lane 9) with ExoIII. Purified DNA was analyzed on a sequencing gel. Nucleosome positions are indicated at left. The DNA marker (M; 10-bp ladder) is in lane 7.



the addition of ACF and ATP, as they did not have space (146 bp) or had reached their ACF-dependent position already (central 248-bp nucleosome). Still, these nucleosomes stimulate the ATPase activity of ISWI and ACF (data not shown). This experimental setup was designed to minimize the background signal of EB cleavage, which would be increased if multiple nucleosome positions and different movement paths would be present.

Nucleosomes were incubated with EB and a combination of ACF and ATP and irradiated for 10 min with the laser. Nucleosomes and free DNA were separated by native gel electrophoresis, isolated from the gel and the distribution of EB-induced DNA nicks was analyzed on sequencing gels. Comparing free DNA and nucleosomes revealed that nucleosomes did not incorporate the intercalating agent, whereas a distribution of single-strand cuts was observed in free DNA (Fig. 5d,

Figure 5 ACF-dependent nucleosome remodeling generates accessible DNA. **(a)** Kinetics of ethidium bromide-dependent DNA cleavage. DNA (1 µg) was incubated with ethidium bromide (EB; 10⁻⁵ M) and irradiated with the laser for the indicated time. The ratio of A₅₁₀ to A₄₂₀ was plotted over time. **(b)** Laser irradiation does not disrupt the nucleosome. Nucleosomes in the presence of ACF and ATP were irradiated with the laser (80 min). Competitor DNA was added and the nucleosomes were analyzed on native polyacrylamide gels. DNA and nucleosome positions are indicated at left. **(c)** Low concentrations of EB do not affect nucleosome remodeling. Purified nucleosomes positioned at the border of the DNA fragment (lane 1) were incubated with ATP, in the absence or presence of ACF (15 fmol) and increasing amounts of EB (10⁻⁷, 10⁻⁶, 10⁻⁵ and 10⁻⁴ M EB; lanes 3–6, 8–11). Reactions were stopped by the addition of competitor DNA and analyzed on native polyacrylamide gels. **(d)** Free DNA and nucleosomes assembled on a 146-bp DNA fragment were incubated with ACF, ATP and EB as indicated. The reaction was irradiated with the laser (10 min), supplemented with competitor DNA and separated on a native gel. DNA and nucleosomes were excised and the purified DNA was analyzed on sequencing gels. The sizes of the 10-bp ladder are indicated at left; the nucleosome (gray oval) and the EB-sensitive sites (triangles) are indicated at right. **(e)** Experiment similar to that described in d. Purified nucleosomes positioned at the center of the 248-bp rDNA fragment were incubated with ATP, ACF and EB as indicated and irradiated with the laser. The nucleosome was isolated and the purified DNA was analyzed on sequencing gels. Lane 4 shows the 10-bp DNA ladder (M). The position of the nucleosome (gray oval) and the EB-sensitive sites (triangles) are indicated.



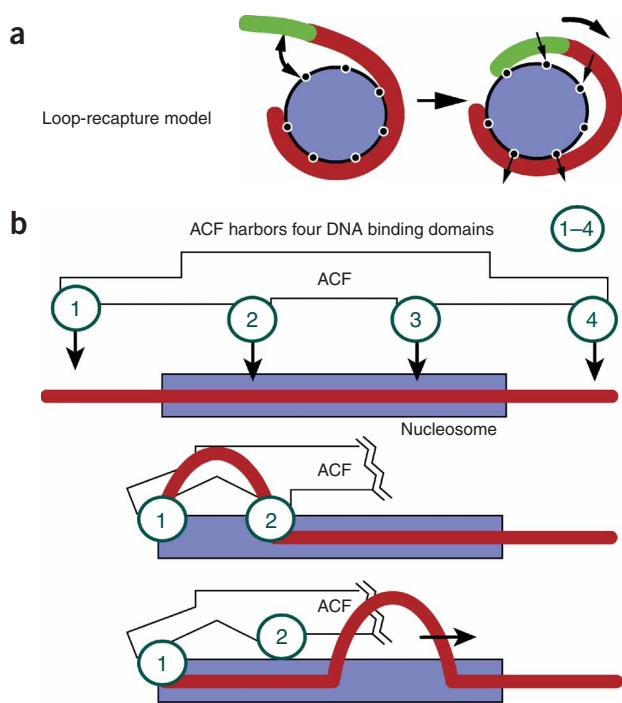


Figure 6 Scheme of the local recapture model. (a) Scheme showing the DNA loop formation on the histone octamer surface. (b) Model for ACF-dependent nucleosome sliding.

1 and 4). However, when ACF was added to the reaction, increased EB-dependent cleavage was observed ~ 20 and ~ 40 bp from the nucleosomal border (lanes 2 and 3). This increased EB sensitivity was ATP-independent and suggests that binding of ACF generated accessible DNA at the nucleosomal extremes. We obtained similar results with the purified 248-bp nucleosomes positioned at the center of the DNA fragment (Fig. 5e). In contrast to the experiments done with the 146-bp nucleosome, the increased DNA accessibility seemed to be weaker, presumably from microheterogeneity of nucleosome positions and the increased degree of possible nucleosome movements on this DNA fragment. We observed an ACF-dependent increase of nucleosome accessibility at the borders of the nucleosome, extending ~ 40 bp into the nucleosome (lanes 2 and 3). Increased EB accessibility in the nucleosome suggests that ACF generates accessible DNA, which is an essential feature of the loop recapture model.

DISCUSSION

In this study we examined the molecular mechanism of nucleosome remodeling by the ISWI-containing ACF chromatin remodeling complexes. In previous experiments we observed that ISWI binds asymmetrically to the nucleosome, thereby moving nucleosomes to the extremes of a linear DNA fragment. In contrast, ACF moved nucleosomes to central positions of the same DNA fragment. Accordingly, we observed symmetrical contact sites of ACF on the nucleosome, in contrast to the single-sided ISWI-nucleosome interaction¹⁸. Contacts of ACF with the nucleosome resemble the interactions of ISWI, γ ISW2 and dNURF with the nucleosome, in that these complexes bind to the DNA linker and the DNA entry-exit sites of the nucleosome^{17,18,31}. ACF-nucleosome interactions extend ~ 40 bp into the nucleosome up to superhelix location 2 (SHL2) and the EB-

binding assay detects ACF-dependent DNA accessibility close to SHL2 (refs. 10,32). The histone H4 tail is required for the ATPase activity of ISWI and the nucleosome crystal structure and cross-linking data suggest that the histone H4 tail interacts with DNA around the SHL2 site^{32–35}. Hence, the proximity of the histone H4 tail with this region is consistent with its critical function in the remodeling process.

The FCCS analysis indicates that ACF consists of a heterotetramer of two ISWI (119 kDa) and two Acl1 (170 kDa) subunits with an apparent molecular mass of 690–730 kDa, similar to CHRAC¹³. In addition, size-exclusion chromatography and glycerol gradients of ACF revealed an apparent complex size of ~ 600 –700 kDa in the absence of DNA. Previously, the molecular mass of ACF was estimated to be between ~ 220 and 400 kDa in glycerol gradients; this would correspond to a heterodimer of one molecule of Acl1 and ISWI^{12,14,36}. However, recent data³⁷ and biochemical experiments (P. Becker, Adolf-Butenandt-Institut, Molekularbiologie, Munich, personal communication) support our findings as they show the presence of more than one ISWI and Acl1 molecules in ACF. The ACF complex harbors four independent DNA-binding sites, whereas only one DNA duplex is bound to ISWI. The FCCS and footprinting data suggest that ACF places two ISWI molecules symmetrically at the DNA entry site of the nucleosome. This remodeler-nucleosome topology would not favor nucleosome repositioning to the borders of the DNA fragment because ISWI could introduce DNA into the nucleosome from either side, eliminating the directionality of nucleosome repositioning. Symmetrical binding of the motor molecules to the DNA entry site would probably position nucleosomes at thermodynamically favored sites. Such a site seems to be the center of the rDNA fragment that contains highly structured DNA³⁸.

The mechanism by which nucleosomes are moved over DNA is still under discussion and the different families of remodeling ATPases may use the same mechanism, irrespective of the different outcomes in various remodeling assays^{2,39}. On one hand, data show the acquisition of DNA twist with all remodeling complexes tested¹⁵. On the other hand, remodeling has been shown not to be affected by DNA nicks and DNA flaps in the path of the moving nucleosome^{16–18}. Although these nucleosome modifications did not have substantial effects, interpretation of the experiments is complicated and a possible role for twist defect diffusion in nucleosome remodeling could not be excluded. However, recent data shows Rsc-dependent nucleosome remodeling on DNA molecules exhibiting gaps in one DNA strand, suggesting a looping mechanism for SWI/SNF-like remodeling complexes⁴⁰. Other studies mapping the increments of nucleosome movements indicate that different classes of ATPases move nucleosomes in steps that are multiples of ~ 10 bp (refs. 17,41,42). In these experiments nucleosome movements in single base pair steps were not observed, which would be expected for a mechanism that involves DNA twisting. However, the fast remodeling kinetics and the asynchronous remodeling reaction pose a challenge for the detection of remodeling intermediates. Therefore we generated modified nucleosomes that allow us to elucidate the remodeling mechanism. Our data exclude a mechanism that involves DNA rotation, because this process would disrupt nucleosomes coupled to magnetic beads.

SWI/SNF-type remodeling complexes have been shown to generate accessible DNA during nucleosome remodeling, whereas DNA accessibility was not obvious for ISWI-containing remodeling complexes³⁹. Here, we applied a novel assay, in which ethidium bromide binding and crosslinking is used to detect a transient site-specific detachment of the nucleosomal DNA. As predicted by the loop recapture model, we observed ACF-dependent incorporation of EB at the borders of the

nucleosome at two regions, overlapping with the ACF-nucleosome interactions. At these sites binding of ACF increased the accessibility of DNA. Thus, for the first time direct evidence is presented that remodelers of the ISWI class remove DNA locally from the nucleosome, indicative of DNA loop formation. Nucleosome remodeling ATPases belong to the helicase superfamily 2 (SF2) suggesting that Snf2p-related ATPases would be ATP-dependent DNA translocases⁴³. Like these, ISWI may bind or hydrolyze ATP at steps subsequent to substrate binding⁴⁴. In agreement with our data, a recent report analyzing the yeast Isw2 complex suggests that ATP is hydrolyzed subsequent to the nucleosome relocation step. The authors conclude that ATP hydrolysis would lead to DNA release from the DNA-binding site of the remodeler and change its conformation to an extended form⁴⁵. This is in agreement with our finding that for ACF both the substrate-binding step and the introduction of the DNA loop do not require ATP.

In summary, the data presented here strongly suggest that nucleosome repositioning by ISWI-containing remodelers follows the loop recapture model (Fig. 6a) Based on the symmetric footprinting pattern, subunit composition of ACF and the FCCS data, we favor a model in which the multiple DNA-binding sites per ACF complex allow the formation of a topological domain. Changing their spatial arrangement upon substrate binding induces the formation of a DNA loop (Fig. 6b). A subsequent coordinated release of the DNA-binding sites would then lead to migration of the DNA loop over the histone octamer surface and result in nucleosome movement.

METHODS

Nucleic acids. Nucleosomes were reconstituted on 146-bp and 248-bp rDNA promoter fragments as described¹⁹. The DNA templates harboring one or two biotins were generated by PCR using biotinylated oligonucleotides. PCR fragments were digested with BamHI and ligated in order to place the biotin at the center of the DNA fragment. The 236-bp DNA fragment containing two central biotins was generated by amplification of an rDNA promoter fragment spanning the sequences from -201 to -78, radioactively labeled at position -201. The oligonucleotide spanning the sequence from -78 to -105 contained a 3' biotin and a BamHI site at position -83. The rDNA fragment was digested with BamHI, purified and the DNA fragments were ligated. The symmetric 236-bp DNA fragment contained two biotin moieties spaced by 44 bp. The DNA fragment containing one biotin moiety was generated with a similar strategy. Two DNA fragments (-232 to -83, one biotin at position -105; -83 to +16) were cleaved with BamHI, purified and ligated. The 248-bp DNA fragment was gel-purified and used for nucleosome assembly.

The 59-bp ES-2 duplexes, covalently labeled via a hexyl linker at the 5' end with 6-carboxyfluorescein (FAM) and/or 6-carboxy-X-rhodamine (ROX), were prepared as described²².

Proteins. Histones, ACF and ISWI were prepared as described²⁰. ACF concentration was determined by measuring the integrated band intensity after Coomassie blue staining on an 8% (w/v) SDS-polyacrylamide gel. The resulting intensity was converted into a protein concentration from a BSA standard curve.

Nucleosome assembly and footprinting analysis. Nucleosome assembly was carried out as described¹⁹. Biotinylated nucleosomes were coupled to magnetic beads (Dyna, Dynabeads M-280 streptavidin) that were equilibrated with EX50 buffer (50 mM KCl, 10 mM Tris-Cl, pH 7.6, 1 mM EDTA, 1.5 mM MgCl₂, 10% (v/v) glycerol, 200 ng μl⁻¹ BSA). Nucleosomes and magnetic beads were incubated on a rotating wheel (10 min, 4 °C), washed with EX70 buffer and directly used for nucleosome remodeling assays. Nucleosome-remodeler interaction assays and DNase I footprinting experiments were done as described¹⁸.

Nucleosome mobility assay and ExoIII mapping. Nucleosome mobility assays were done as described¹⁹. Remodeling reactions containing bead-bound nucleosomes were stopped by the addition of 500 ng circular competitor DNA. The reaction was incubated with 400 U ml⁻¹ ExoIII for 2 min at 30 °C.

The reactions were stopped by the addition of 0.25 volume stop buffer (4% (w/v) SDS, 40 mM EDTA), incubated with 20 μg proteinase K for 1 h at 37 °C, and DNA was extracted with phenol according to standard procedures and analyzed on sequencing gels.

Ethidium bromide intercalation assay. About 1 pmol of the purified nucleosomes was incubated with EB at a final concentration of 5×10^{-7} M. The ACF concentration was adjusted according to electromobility shift assays with the 248-bp nucleosome, yielding ~50% ACF-nucleosome complexes. A 100-μl reaction mixture was placed in siliconized, transparent Eppendorf vials and irradiated for 10 min with an Argon ion laser (Model 177; 100 mW; Spectra Physics) tuned to 488 nm. Reactions were stopped by the addition of competitor DNA, loaded on preparative polyacrylamide gels and free DNA and nucleosomes were isolated. DNA was extracted and analyzed on sequencing gels.

Fluorescence correlation spectroscopy. FCS and FCCS measurements were carried out at room temperature with a FCS2 extension attached to a Leica TCS SP2 AOBs confocal laser scanning microscope (Leica Microsystems). We used the 488-nm line of the Ar laser for FAM and the 594-nm line of a HeNe or the 561-nm line of a diode laser for ROX excitation. Incident laser power was set to a few kilowatts per square centimeter in the sample. Fluorescence was separated from the laser light with the AOBs beam splitter and distributed spectrally with band pass filters into two channels (500–550 nm for FAM and 608–672 nm for ROX) equipped with avalanche photodiodes for photon counting. The focus of an HCXPLApo CS 63 × 1.2 WCorr water immersion objective lens was placed into the solution to be analyzed 20–30 μm above the upper coverslide surface.

Titration and control experiments were conducted in 4 mM Tris-HCl, pH 7.6, 0.2 mM MgCl₂, 50 mM KCl, 2% (v/v) glycerol, 0.2 mM DTT and 0.05% (v/v) Igepal C-620 (Sigma-Aldrich, Taufkirchen) in a 40 μl reaction volume. ACF was added to an equimolar solution of ES-2_r and ES-2_l (20 nM each). The salt concentration was increased to 0.3 mM MgCl₂ and 70 mM KCl at the titration end point as the protein stock solution contained 250 mM NaCl and 1 mM MgCl₂, in which ACF was found to be more stable. For each sample, three to five measurements of 60 s were taken. The experiments with ISWI were conducted under the same conditions as described above for ACF. Auto- and cross-correlations were acquired, processed and evaluated using the Leica/ISS FCS software. Global fitting of analytical correlation functions using the Marquardt-Levenberg algorithm was conducted as described in **Supplementary Methods**.

Accession codes. Bind identifiers (<http://bind.ca>): 300963, 300964 and 300965.

Note: Supplementary information is available on the Nature Structural & Molecular Biology website.

ACKNOWLEDGMENTS

We thank H. Emmerichs from Spectra Physics for providing the laser equipment and Leica Microsystems for making the FCS system available. This work was supported by grants from Deutsche Forschungsgemeinschaft and the Volkswagen Foundation in the program Junior Research Groups at German Universities.

COMPETING INTERESTS STATEMENT

The authors declare that they have no competing financial interests.

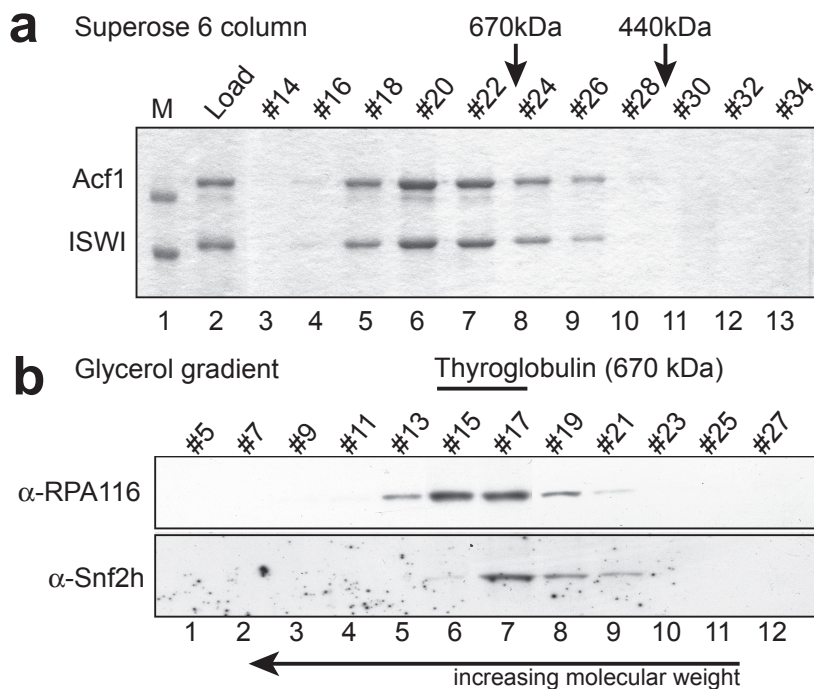
Received 22 March; accepted 23 June 2005

Published online at <http://www.nature.com/nsmb>

1. Becker, P.B. & Hörz, W. ATP-dependent nucleosome remodeling. *Annu. Rev. Biochem.* **71**, 247–273 (2002).
2. Längst, G. & Becker, P.B. Nucleosome remodeling: one mechanism, many phenomena? *Biochim. Biophys. Acta* **1677**, 58–63 (2004).
3. Widom, J. Role of DNA sequence in nucleosome stability and dynamics. *Q. Rev. Biophys.* **34**, 269–324 (2001).
4. Van Holde, K.E. & Yager, T.D. Nucleosome motion: evidence models. in *Structure and Function of the Genetic Apparatus* (eds. Nicolini, C. & Ts'o, P.O.P.) (Plenum, New York, 1985).
5. Schiessel, H., Widom, J., Bruinsma, R.F. & Gelbart, W.M. Polymer reptation and nucleosome repositioning. *Phys. Rev. Lett.* **86**, 4414–4417 (2001).
6. Widom, J. Structure, dynamics, and function of chromatin *in vitro*. *Annu. Rev. Biophys. Biomol. Struct.* **27**, 285–327 (1998).

7. Studitsky, V.M., Clark, D.J. & Felsenfeld, G. A histone octamer can step around a transcribing polymerase without leaving the template. *Cell* **76**, 371–382 (1994).
8. Li, G., Levitus, M., Bustamante, C. & Widom, J. Rapid spontaneous accessibility of nucleosomal DNA. *Nat. Struct. Mol. Biol.* **12**, 46–53 (2005).
9. Brower-Toland, B.D. *et al.* Mechanical disruption of individual nucleosomes reveals a reversible multistage release of DNA. *Proc. Natl. Acad. Sci. USA* **99**, 1960–1965 (2002).
10. Davey, C.A., Sargent, D.F., Luger, K., Maeder, A.W. & Richmond, T.J. Solvent mediated interactions in the structure of the nucleosome core particle at 1.9 Å resolution. *J. Mol. Biol.* **319**, 1097–1113 (2002).
11. Tsukiyama, T., Daniel, C., Tamkun, J. & Wu, C. ISWI, a member of the SWI2/SNF2 ATPase family, encodes the 140 kDa subunit of the nucleosome remodeling factor. *Cell* **83**, 1021–1026 (1995).
12. Ito, T., Bulger, M., Pazin, M.J., Kobayashi, R. & Kadonaga, J.T. ACF, an ISWI-containing and ATP-utilizing chromatin assembly and remodeling factor. *Cell* **90**, 145–155 (1997).
13. Varga-Weisz, P. *et al.* Chromatin-remodelling factor CHRAC contains the ATPases ISWI and topoisomerase II. *Nature* **388**, 598–602 (1997).
14. Ito, T. *et al.* ACF consists of two subunits, Acf1 and ISWI, that function cooperatively in the ATP-dependent catalysis of chromatin assembly. *Genes Dev.* **13**, 1529–1539 (1999).
15. Havas, K. *et al.* Generation of superhelical torsion by ATP-dependent chromatin remodeling activities. *Cell* **103**, 1133–1142 (2000).
16. Aoyagi, S. & Hayes, J.J. hSWI/SNF-catalyzed nucleosome sliding does not occur solely via a twist-diffusion mechanism. *Mol. Cell. Biol.* **22**, 7484–7490 (2002).
17. Schwanbeck, R., Xiao, H. & Wu, C. Spatial contacts and nucleosome step movements induced by the NURF chromatin remodeling complex. *J. Biol. Chem.* **279**, 39933–39941 (2004).
18. Längst, G. & Becker, P.B. ISWI induces nucleosome sliding on nicked DNA. *Mol. Cell* **8**, 1085–1092 (2001).
19. Längst, G., Bonte, E.J., Corona, D.F. & Becker, P.B. Nucleosome movement by CHRAC and ISWI without disruption or trans-displacement of the histone octamer. *Cell* **97**, 843–852 (1999).
20. Eberharter, A. *et al.* Acf1, the largest subunit of CHRAC, regulates ISWI-induced nucleosome remodelling. *EMBO J.* **20**, 3781–3788 (2001).
21. Rigler, R. & Elson, E.S. *Fluorescence Correlation Spectroscopy: Theory and Applications* (Springer, Berlin, 2001).
22. Rippe, K. Simultaneous binding of two DNA duplexes to the NtrC-enhancer complex studied by two-color fluorescence cross-correlation spectroscopy. *Biochemistry* **39**, 2131–2139 (2000).
23. Weidemann, T., Wachsmuth, M., Tewes, M., Rippe, K. & Langowski, J. Analysis of ligand binding by two-colour fluorescence cross-correlation spectroscopy. *Single Molecules* **3**, 49–61 (2002).
24. Schwille, P., Meyer-Almes, F.J. & Rigler, R. Dual-color fluorescence cross-correlation spectroscopy for multicomponent diffusional analysis in solution. *Biophys. J.* **72**, 1878–1886 (1997).
25. Rippe, K., Mucke, N. & Schulz, A. Association states of the transcription activator protein NtrC from *E. coli* determined by analytical ultracentrifugation. *J. Mol. Biol.* **278**, 915–933 (1998).
26. McMurray, C.T. & van Holde, K.E. Binding of ethidium bromide causes dissociation of the nucleosome core particle. *Proc. Natl. Acad. Sci. USA* **83**, 8472–8476 (1986).
27. McMurray, C.T. & van Holde, K.E. Binding of ethidium to the nucleosome core particle. 1. Binding and dissociation reactions. *Biochemistry* **30**, 5631–5643 (1991).
28. Deniss, I.S. & Morgan, A.R. Studies on the mechanism of DNA cleavage by ethidium. *Nucleic Acids Res.* **3**, 315–323 (1976).
29. Krishnamurthy, G., Polte, T., Rooney, T. & Hogan, M.E. A photochemical method to map ethidium bromide binding sites on DNA: application to a bent DNA fragment. *Biochemistry* **29**, 981–988 (1990).
30. Boles, T.C. & Hogan, M.E. Site-specific carcinogen binding to DNA. *Proc. Natl. Acad. Sci. USA* **81**, 5623–5627 (1984).
31. Kagalwala, M.N., Glaus, B.J., Dang, W., Zofall, M. & Bartholomew, B. Topography of the ISW2–nucleosome complex: insights into nucleosome spacing and chromatin remodeling. *EMBO J.* **23**, 2092–2104 (2004).
32. Luger, K., Mader, A.W., Richmond, R.K., Sargent, D.F. & Richmond, T.J. Crystal structure of the nucleosome core particle at 2.8 Å resolution. *Nature* **389**, 251–260 (1997).
33. Clapier, C.R., Längst, G., Corona, D.F., Becker, P.B. & Nightingale, K.P. Critical role for the histone H4 N terminus in nucleosome remodeling by ISWI. *Mol. Cell. Biol.* **21**, 875–883 (2001).
34. Clapier, C.R., Nightingale, K.P. & Becker, P.B. A critical epitope for substrate recognition by the nucleosome remodeling ATPase ISWI. *Nucleic Acids Res.* **30**, 649–655 (2002).
35. Ebralidse, K.K., Grachev, S.A. & Mirzabekov, A.D. A highly basic histone H4 domain bound to the sharply bent region of nucleosomal DNA. *Nature* **331**, 365–367 (1988).
36. LeRoy, G., Loyola, A., Lane, W.S. & Reinberg, D. Purification and characterization of a human factor that assembles and remodels chromatin. *J. Biol. Chem.* **275**, 14787–14790 (2000).
37. Poot, R.A. *et al.* HuCHRAC, a human ISWI chromatin remodelling complex contains hACF1 and two novel histone-fold proteins. *EMBO J.* **19**, 3377–3387 (2000).
38. Längst, G., Schatz, T., Langowski, J. & Grummt, I. Structural analysis of mouse rDNA: coincidence between nuclease hypersensitive sites, DNA curvature and regulatory elements in the intergenic spacer. *Nucleic Acids Res.* **25**, 511–517 (1997).
39. Flaus, A. & Owen-Hughes, T. Mechanisms for ATP-dependent chromatin remodelling: farewell to the tuna-can octamer? *Curr. Opin. Genet. Dev.* **14**, 165–173 (2004).
40. Lorch, Y., Davis, B. & Kornberg, R.D. Chromatin remodeling by DNA bending, not twisting. *Proc. Natl. Acad. Sci. USA* **102**, 1329–1332 (2005).
41. Kassabov, S.R., Zhang, B., Persinger, J. & Bartholomew, B. SWI/SNF unwraps, slides, and rewraps the nucleosome. *Mol. Cell* **11**, 391–403 (2003).
42. Flaus, A. & Owen-Hughes, T. Dynamic properties of nucleosomes during thermal and ATP-driven mobilization. *Mol. Cell. Biol.* **23**, 7767–7779 (2003).
43. Flaus, A. & Owen-Hughes, T. Mechanisms for ATP-dependent chromatin remodelling. *Curr. Opin. Genet. Dev.* **11**, 148–154 (2001).
44. Singleton, M.R. & Wigley, D.B. Modularity and specialization in superfamily 1 and 2 helicases. *J. Bacteriol.* **184**, 1819–1826 (2002).
45. Fitzgerald, D.J. *et al.* Reaction cycle of the yeast Isw2 chromatin remodeling complex. *EMBO J.* **23**, 3836–3843 (2004).

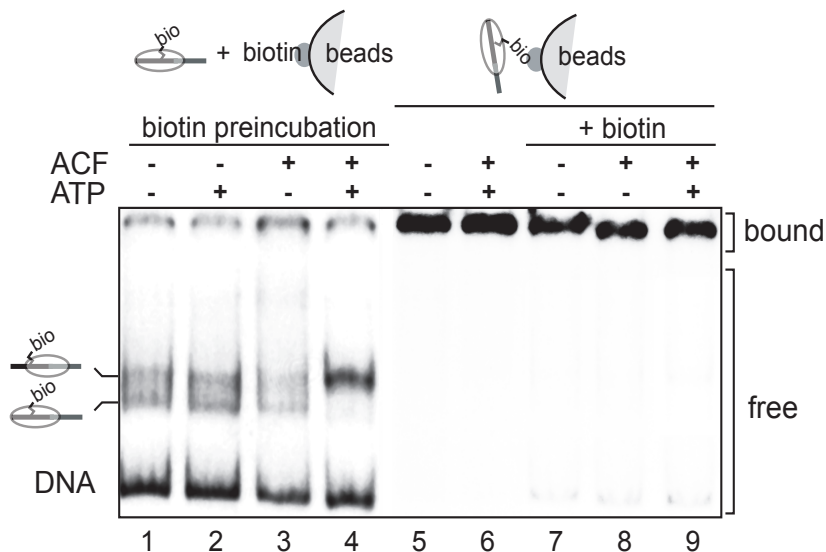
Supplementary Figure 1 ACF has an apparent molecular mass above 600 kDa



Supplementary Figure 1 Estimation of the molecular mass of ACF using gel filtration and glycerol gradient. **(a)**, Recombinant ACF (lane 1, Load) was subjected to a Superose 6 gel filtration column, fractions were collected, loaded on a 6% SDS-PAGE as indicated and stained with coomassie blue. The positions of the Thyroglobulin (670 kDa) and Apoferritin (440 kDa) are indicated. **(b)**, Mouse nuclear extract was fractionated on a glycerol gradient (5-45%) and individual fractions were separated on a 6% SDS-PAGE. RPA116, a subunit of RNA Polymerase I (the core polymerase is migrating at 660 kDa) and Snf2h were detected by western blot. No smaller Snf2h complexes were detected in the glycerol gradient. The position of the Thyroglobulin marker is indicated.

Supplementary Figure 2 Nucleosome remodeling does not release biotinylated nucleosomes from Streptavidin beads.

It could be envisioned that the ATPase activity of ACF or the nucleosome remodeling mechanism would lead to a transient displacement of the nucleosome from the Streptavidin beads followed by immediate rebinding of the nucleosome. In order to exclude this possibility, we performed the nucleosome remodeling reactions in the presence of free biotin that would compete with the potentially released nucleosomes for the Streptavidin binding sites. Streptavidin beads were incubated with Biotin prior to the addition of nucleosomes, ACF and ATP to test the efficiency of ACF dependent nucleosome remodeling. At these conditions, nucleosomes were quantitatively moved to the central DNA position by ACF (Fig. S2, lanes 1 to 4). Preincubation of the nucleosomes with the Streptavidin beads resulted in quantitative binding without nucleosome release in the presence of ATP and ACF (lanes 5 and 6). The addition of free Biotin as a competitor did not promote an ACF/ATP dependent release of the bead bound nucleosomes (lanes 7 to 9). This experiment indicates that during the ACF dependent remodeling reaction nucleosomes were not detached from the beads.



Supplementary Figure 2 Nucleosome remodeling does not preferentially release bead bound nucleosomes. Nucleosomes (100 fmol) assembled on internally biotinylated DNA were used for nucleosome remodeling reactions in the presence of free Biotin (20 pmol). Streptavidin magnetic beads were incubated with Biotin before (lanes 1 to 4) or after (lanes 7 to 9) the addition of the radioactively labeled, biotinylated nucleosomes. Nucleosomes were incubated with ACF (20 fmol) for 20 min in the presence or absence of ATP and then loaded on native polyacrylamide gels. Free DNA, nucleosomes and the bead bound nucleosomes are indicated.

Supplementary Methods

Fluorescence correlation spectroscopy (FCS) is a method that analyses the fluorescence fluctuations from sparse molecules diffusing into and out of a spatially fixed microscopic volume (for review see ref. ¹). This observation volume is defined by a confocal fluorescence excitation and detection setup like that of a confocal laser scanning microscope. In a solution of fluorescently labeled molecules, the signal arises from fluctuations in the number of particles in the observation volume due to their 3D Brownian motion. An autocorrelation analysis of the signal $F_i(t)$ in the detection channel $i = 1$ or 2 yields the mean dwell time or diffusion correlation time $\tau_D \propto 1/D$ of the molecules in the focus, which is the decay time of the correlation function and which is inversely proportional to the diffusion coefficient D , and gives their number N represented by the inverse of the amplitude of the correlation function:

$$G'_{\text{auto},i}(\tau) = \frac{\langle F_i(t)F_i(t+\tau) \rangle^2}{\langle F_i(t) \rangle^2} - 1 = \frac{1}{N} \left(1 + \frac{\tau}{\tau_D}\right)^{-1} \left(1 + \frac{\tau}{\kappa^2 \tau_D}\right)^{-1/2} \quad (\text{eq. 1})$$

Here, κ characterizes the elongation of the focus along the optical axis. For studies on binding or complex formation, it must be possible to distinguish free and bound species in terms of their diffusion properties by fitting a sum of analytical correlation functions to the data:

$$G'_{\text{auto},i}(\tau) = \frac{1}{N} \sum_{\text{species } s} \rho_s \left(1 + \frac{\tau}{\tau_{D,s}}\right)^{-1} \left(1 + \frac{\tau}{\kappa^2 \tau_{D,s}}\right)^{-1/2} \quad (\text{eq. 2})$$

where ρ_s stands for the molar fraction of species s . In most cases, additional fluctuations like triplet state kinetics with a characteristic lifetime τ_{trip} of the fluorophores occur that must be accounted for by an additional time-dependent factor:

$$G_{\text{auto},i}(\tau) = \left[1 + \beta \exp\left(-\frac{\tau}{\tau_{\text{trip}}}\right)\right] G'_{\text{auto},i}(\tau), \quad (\text{eq. 3})$$

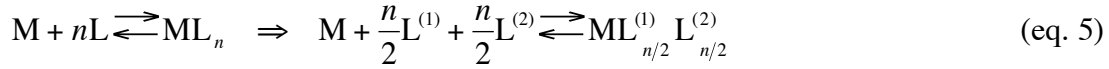
i.e., $G'_{\text{auto},i}(0)$ is the correlation amplitude after triplet correction.

A more sensitive approach is based on a two-color setup where different species and ligand binding be analyzed on the basis of spectrally different labels by splitting their signals into two different detection

channels with signals $F_1(t)$ and $F_2(t)$ ¹⁻⁴. A temporal cross correlation analysis of the signals allows to collect information exclusively about complexes carrying both types of dyes:

$$G_{\text{cross}}(\tau) = G'_{\text{cross}}(\tau) = \frac{\langle F_1(t)F_2(t+\tau) \rangle^2}{\langle F_1(t) \rangle \langle F_2(t) \rangle} - 1 = \frac{1}{N} \left(1 + \frac{\tau}{\tau_D} \right)^{-1} \left(1 + \frac{\tau}{\kappa^2 \tau_D} \right)^{-1/2} \quad (\text{eq. 4})$$

This method can be used to study complex formation or multimerization as described recently^{2,3}. When a macromolecule M is expected to bind an unknown number n of ligands L , it is a suitable approach to label equimolar fractions of L with two different dyes of type $i = 1$ and 2 each of which is assigned to one detection channel:



The occupation probability of each binding site on M for $L^{(1)}$ or $L^{(2)}$, respectively, determines whether the equilibrium is biased more to the right-hand or to the left-hand side and is quantified using p with $0 \leq p \leq 0.5$. Statistical considerations and the definitions of the correlation functions lead to expressions for the correlation amplitudes after triplet correction in the absence of free ligands²:

$$G'_{\text{auto},i}(0) = \frac{1}{N_M} \left(1 - \frac{1}{n} + \frac{1}{np} \right) \quad (\text{eq. 6})$$

$$G'_{\text{cross}}(0) = \frac{1}{N_M} \left(1 - \frac{1}{n} \right)$$

The autocorrelation function yields an apparent number of bound ligands $N_{L, \text{bound}}^{\text{app}(i)} = N_M / (1 - 1/n + 1/np)$. In the additional presence of free ligand molecules $N_{L, \text{free}}^{(i)} = N_{L, \text{total}}^{(i)} - N_M np$, one can observe an apparent fraction of bound molecules

$$\rho_{\text{bound}}^{\text{app}(i)} = \frac{N_{L, \text{bound}}^{\text{app}(i)}}{N_{L, \text{bound}}^{\text{app}(i)} + N_{L, \text{free}}^{(i)}} = \left[1 + \left(1 - \frac{1}{n} + \frac{1}{np} \right) \left(\frac{N_{L, \text{total}}^{(i)}}{N_M} - np \right) \right]^{-1}, \quad (\text{eq. 7})$$

and the correlation amplitudes are extended to

$$\begin{aligned}
G'_{\text{auto},i}(0) &= \frac{1}{N_{L,\text{bound}}^{\text{app}(i)} + N_{L,\text{free}}^{(i)}} = \frac{1}{N_M} \left(\frac{N_{L,\text{total}}^{(i)}}{N_M} - np + \frac{1}{1 - 1/n + 1/np} \right)^{-1} \\
G'_{\text{cross}}(0) &= \frac{1}{N_M} \left(1 - \frac{1}{n} \right) \frac{\langle F_{1,\text{bound}} \rangle}{\langle F_{1,\text{bound}} + F_{1,\text{free}} \rangle} \frac{\langle F_{2,\text{bound}} \rangle}{\langle F_{2,\text{bound}} + F_{2,\text{free}} \rangle} = \frac{1}{N_M} \left(1 - \frac{1}{n} \right) \left(\frac{N_M np}{N_{L,\text{total}}^{(i)}} \right)^2
\end{aligned} \tag{eq. 8}$$

where $F_{i,\text{bound}} \propto N_M np$ and $F_{i,\text{bound}} + F_{i,\text{free}} = F_{i,\text{total}} \propto N_{L,\text{total}}^{(i)}$ are the signal contributions in channel i for only the bound and for all ligand molecules, respectively. Computing the *ratioG*, which is the amplitude of the cross-correlation function $G'_x(0)$ divided by the geometric mean of both autocorrelation function amplitudes cancels out dilution-related changes and yields an appropriate observable for FCCS studies:

$$\text{ratio}G = \frac{G'_{\text{cross}}(0)}{\sqrt{G'_{\text{auto},1}(0)G'_{\text{auto},2}(0)}} = \left[\left(1 - \frac{1}{n} \right) \left(\frac{N_{L,\text{total}}^{(i)}}{N_M} - np \right) + \frac{n-1}{n-1+1/p} \left(\frac{N_M np}{N_{L,\text{total}}^{(i)}} \right) \right]^2 \tag{eq. 9}$$

It is important to note that all particle numbers N can be transformed directly into concentrations c by dividing all numbers by the observation volume, $c = N/V_{\text{obs}}$. The value of *ratioG* increases with the fraction of molecules that carry both fluorescent dyes simultaneously and its maximum value depends on the number n of binding sites. For an equimolar mixture of two ligands labeled in different colors the maximum is given by $(n-1)/(n+1)$. Thus, for a complex that has $n = 2$ binding sites it would be 0.33 in the absence of free ligand, since complexes are formed that have either two red or two green labels. Any free DNA ligand would further reduce the value of *ratioG* according to eq. 9. The corresponding values for $n = 3$ and $n = 4$ would be 0.5 and 0.6, respectively, and the maximum of *ratioG* approaches 1 for large n . For physical reasons, the theoretical minimum and maximum values of 0 and 1 for *ratioG* cannot be obtained experimentally. Therefore, the instrumental setup was calibrated with reference samples that contain increasing amounts of double-labeled ES-2_{fr} mixed with the single-labeled ES-2_f and ES-2_r to determine the corrected value $\text{ratio}G_{\text{cor}}^{2,3}$. The linear regression of the data presented in **Fig. 2b** yielded values of $\text{ratio}G_{\text{min}} = 0.040 \pm 0.001$ and of $\text{ratio}G_{\text{max}} = 0.548 \pm 0.008$ corresponding to the normalized values of 0 and 1 for $\text{ratio}G_{\text{cor}}$ according to eq. 10.

$$\text{ratio}G_{\text{cor}} = \frac{\text{ratio}G_{\text{exp}} - \text{ratio}G_{\text{min}}}{\text{ratio}G_{\text{max}} - \text{ratio}G_{\text{min}}}. \tag{eq. 10}$$

From the law of mass action and the definition of the microscopic dissociation constant K_d for the binding of ligand L to an isolated binding site on complex M , the probability p that this site is occupied by a ligand with label i , $L^{(i)}$, can be calculated as a function of the complex concentration c_M :

$$p = \frac{c_M n + L_{\text{total}}^{(i)} + K_d - \sqrt{(c_M n + L_{\text{total}}^{(i)} + K_d)^2 - 4 c_M n L_{\text{total}}^{(i)}}}{4 c_M n}. \quad (\text{eq. 11})$$

For an unknown composition of the basic complex M , its concentration can be expressed in the titration experiments in terms of j subunits at a concentration c_U which then bind n ligand molecules L in total. The complex concentration is given as:

$$c_M = \frac{c_U}{j}. \quad (\text{eq. 12})$$

In the titration experiments, the protein complex M expressed in terms of the concentration of subunits c_U is added gradually to a given equimolar mixture of ligand L with two different labels. Thus, one obtains two auto- and one cross correlation curve for every concentration step. A fit of the data to eqs. 3 and 4 yields the amplitudes and thus *ratioG* as a function of the complex subunit concentration c_U . After introducing eq. 11 and eq. 12 into eq. 9, the resulting expression can be fit to the experimental *ratioG* values and allows it to derive the number j of subunits per complex M , the number of binding sites n on the complex, and the microscopic dissociation constant K_d .

During the titrations the ionic strength I was increased from 0.2 mM MgCl₂ and 50 mM KCl ($I = 0.065$ M) at the beginning to 0.3 mM MgCl₂ and 70 mM KCl ($I = 0.085$ M) at the titration end point as ACF was added from a protein stock solution containing 250 mM NaCl and 1 mM MgCl₂, in which it was found to be more stable. This led to a slight reduction of the binding affinity, since the dissociation constant for ACF-DNA binding was found to be dependent on the ionic strength. From FCCS measurements at 60, 85, 110 and 135 mM KCl concentrations a plot of $\log(K_d)$ versus the log of the ionic strength I was derived. It displayed an apparent linear relation with a slope $\Delta\log(K_D)/\Delta\log(I) \sim 10$ as reported previously for the unspecific DNA binding of other proteins⁵. Including the salt dependence into the fit function also yielded values of $j \approx 2$ and $n \approx 4$ and did not improve the fit.

References

1. Rigler, R. & Elson, E.S. *Fluorescence correlation spectroscopy: theory and applications*, (Springer, Berlin, 2001).
2. Weidemann, T., Wachsmuth, M., Tewes, M., Rippe, K. & Langowski, J. Analysis of ligand binding by two-colour fluorescence cross-correlation spectroscopy. *Single Mol.* **3**, 49-61 (2002).
3. Rippe, K. Simultaneous binding of two DNA duplexes to the NtrC-enhancer complex studied by two-color fluorescence cross-correlation spectroscopy. *Biochemistry* **39**, 2131-2139 (2000).
4. Schwille, P., Meyer-Almes, F.J. & Rigler, R. Dual-color fluorescence cross-correlation spectroscopy for multicomponent diffusional analysis in solution. *Biophys. J.* **72**, 1878-1886 (1997).
5. Record, M.T., Jr., Zhang, W. & Anderson, C.F. Analysis of effects of salts and uncharged solutes on protein and nucleic acid equilibria and processes: a practical guide to recognizing and interpreting polyelectrolyte effects, Hofmeister effects, and osmotic effects of salts. *Adv Protein Chem* **51**, 281-353 (1998).